Journal of Water Process Engineering 68 (2024) 106300

Contents lists available at ScienceDirect

Journal of Water Process Engineering

journal homepage: www.elsevier.com/locate/jwpe

Sintered glass filter as a membrane impregnated with g-C_3N_4 and AuAg/g-C_3N_4 to degrade Rhodamine B with application in decentralized areas

Leticia Santamaría [a,c,*], Lyda Patricia Sabogal-Paz [b], Bárbara Luíza Souza Freitas [b], Maria Teresa Hoffmann [b], David Royo-Pareja [a], José M. López-de-Luzuriaga [a], Miguel Monge [a,**]

[a] Departamento de Química, Instituto de Investigación en Química de la Universidad de La Rioja (IQUR), C/ Madre de Dios 53, E-26006 Logroño, La Rioja, Spain
[b] Department of Hydraulics and Sanitation, São Carlos School of Engineering, University of São Paulo, Avenida Trabalhador São-Carlense, 400, São Carlos, São Paulo 13566-590, Brazil
[c] INAMAT^2,-Departamento de Ciencias, Edificio de los Acebos, Universidad Pública de Navarra, Campus de Arrosadía, E-31006 Pamplona, Spain

ARTICLE INFO

Editor: Andreina García

Keywords:
Photocatalysis
Carbon nitride
Nanoparticles
Sustainable development goals
Water supply
Costs

ABSTRACT

This work shows a novel approach utilizing graphitic carbon nitride (g-C_3N_4) deposited on a sintered glass filter as a membrane enhanced with gold-silver nanoparticles for the removal of emerging pollutants. g-C_3N_4 was synthesized directly onto the membrane surface with a simple vapor deposition method. Membranes with two different porosities, g-C_3N_4 and the noble-metal nanoparticles were put to the test by exploring their photocatalytic capacity to degrade rhodamine B dye (RhB). FT-IR, PL, SEM, EDX and DRS characterization techniques were performed to analyse the catalysts. RhB degradation was tested in static (i.e. petri dish) and dynamic conditions (i.e. photocatalytic membrane setup). Filtered volumes, turbidity effect and stability were tested in dynamic conditions for the membrane that had the greatest potential for full-scale use. The results confirm the efficient RhB degradation capacity of the catalysts, highlighting the potential of this proposed setup; however, the cost of technology for decentralized areas is still an impediment. These findings not only contribute to advancing the understanding of pollutant removal technologies, but also, offer practical insights into the future deployment of such systems on a larger scale.

1. Introduction

Even though developed countries have successfully used extensive centralized water treatment systems, the transference of this technology to emergent nations and decentralized areas can be severely limited [1] and this is one of the reasons for a constant search for efficient and low-cost technologies, compatible for limited contexts.

Efforts have been recently concentrated on developing visible light responsive photocatalysts to efficiently harvest solar visible light. In this context, the use of graphitic carbon nitride (g-C_3N_4) has been gaining attention in the last decade due to its remarkable properties [2], such as low band gap (2.7 eV), which makes it suitable for visible light absorption, chemical stability and easy synthesis procedure. Nevertheless, some drawbacks have to be overcome to make it more efficient, i.e. a high photoinduced electron-hole recombination rate, a very narrow visible-light absorption capacity or a low specific surface area [3–5].

g-C_3N_4 performance has been proven to greatly improve with the deposition of noble metal nanoparticles (NPs), such as gold (Au), silver (Ag) or platinum (Pt), to ameliorate the electron-hole charge separation [6,7]. These NPs bring light absorption in the visible or near-infrared light (NIR) range to the binary system.

The localized surface plasmon resonance effect (LSRP) is an optical phenomenon that appears if the size of the NPs is much smaller than the incident wavelength [8]. In LSRP, coherent oscillation of the conduction band electrons is caused by interaction with the electromagnetic field which cuts out to a great extend electron-hole recombination [9–11]. The noble metal NPs also form a heterojunction with the semiconductor, called the Schottky barrier that sets up a transfer of the photo-mobilized electrons in the semiconductor and improves the charge carrier separation [12,13]. In addition, the hot electrons excited by light in the plasmonic nanoparticles can also be transferred to the conduction band of the semiconductor, producing a charge carrier separation in the

* Correspondence to: L. Santamaría, INAMAT^2,-Departamento de Ciencias, Edificio de los Acebos, Universidad Pública de Navarra, Campus de Arrosadía, E-31006 Pamplona, Spain.
** Corresponding author.
E-mail addresses: lesanta@unirioja.es (L. Santamaría), miguel.monge@unirioja.es (M. Monge).

https://doi.org/10.1016/j.jwpe.2024.106300
Received 3 June 2024; Received in revised form 2 October 2024; Accepted 6 October 2024
Available online 19 October 2024

nanoparticle.

g-C_3N_4 directly deposited on a surface with a simple and effective method is also useful for practical applications; there is no need to recover the g-C_3N_4 after each use as the photocatalyst stays fixed to the membrane's surface. In addition, it favours a better dispersion of the catalyst and, as the contaminant solution slowly passes through the membrane, it assures the pollutant-catalyst contact without the need for stirring.

In order to assess the efficiency of both the catalyst and the device in which is placed, rhodamine B (RhB) was chosen as a pollutant in our work. RhB is a fluorescent dye often used as hydrological tracer to examine flow pathways and pollutant dispersal in groundwater inside the water supply catchment areas. Tracing tests with dyes may represent a risk of long-term contamination in the studied aquifer as, it is considered potentially genotoxic and carcinogenic, and after its treatment, it can generate by-products [14]. The assessment of the aquatic toxicity and environmental safety of RhB as a tracer compound concluded that, for no risks of effects in freshwater, continuous discharges must not exceed 14 μg/L and intermittent discharge 140 μg/L [15].

In this context, we report the synthesis of a nanocomposite with g-C_3N_4 that has been placed on the surface of a sintered glass filter as a membrane with different porosities via a simple deposition method. The addition of bimetallic AuAg NPs was also examined and the nanocomposite efficiency for the degradation of RhB was measured in both visible and solar light. The membrane was placed in a device to evaluate its ability to filter and photocatalyze. Additionally, a photocatalyst-membrane reactor was designed, and the costs were evaluated to estimate its sustainability in decentralized areas. Overall, the novelty of this study consists of the development of the integral fabrication of a device for decentralized wastewater treatment, starting from the design of new plasmonic photocatalysts, their implementation in sintered glass membranes, and the design of a device for their practical use.

2. Experimental procedure

2.1. Materials

Melamine (99 %, Acros Organics) was utilized for g-C_3N_4 synthesis. Precursors [AuCl(tht)] (tht = tetrahydrothiophene), [NBu_4][Au(C_6F_5)$_2$], $AgClO_4$ and [$Au_2Ag_2(C_6F_5)_4(OEt_2)]_n$ were used for the synthesis of Au—Ag bimetallic nanoparticles on g-C_3N_4 [16–18] (see Supplementary material). Two types of Robuglas® commercial sintered glass filters with Ø = 2.0 cm were tested as membranes with porosity 2 (i.e. 40–100 μm) and porosity 3 (i.e. 16–40 μm). Kaolin (Sigma-Aldrich, K7375) was employed to prepare the studied water with turbidity. RhB (>95 %, Sigma-Aldrich), triisopropylsilane (TIPS, 98 %, Sigma-Aldrich), tetrahydrofuran (HPLC grade, VWR Chemicals) were used without further modification.

2.2. Synthesis procedure of sintered glass filters as membranes impregnated with g-C_3N_4

1.0 g of melamine was loaded on top of the membranes described in the previous section and placed in a crucible. The crucible was then covered with aluminium foil to prevent the sublimation of the precursor and afterwards they were placed in a muffle (Nabertherm, B410) at 500 °C for 2 h and 2 h more at 520 °C (Image S1 - Supplementary material). At the end, the membranes were thoroughly washed and dried (80 °C for 10 h). g-C_3N_4 powder that has not adhered to the membrane surface was collected for comparison purposes by different characterization techniques.

2.3. Synthesis procedure of sintered glass filters as membranes impregnated with AuAg/g-C_3N_4

Membranes were weighed to define the amount of impregnated g-C_3N_4. From there, 5 % by weight of AuAg nanoparticles was calculated for each sample. The membranes were placed in a beaker with 10 mL of THF and 20 mg of $[Au_2Ag_2(C_6F_5)_4(OEt_2)]_n$ dissolved and gently stirred for 30 min, acquiring a bright orange colour (Image S2 - Supplementary material). They were then removed from the beaker and allowed to dry to air and placed in a new beaker with 10 mL of THF at 70 °C. After that, 0.5 mL of TIPS was added, and the membranes were left in the beaker for 5 min under gentle agitation. They were removed and allowed to air dry. Their final surface colour was purple (Image S2 - Supplementary material). The presence of both the g-C_3N_4 and the AuAg NPs adhered to the membranes are evidenced in Image S3 (Supplementary material), showing a different fluorescence when illuminated with a UV lamp (λ = 365 nm).

2.4. Characterization g-C_3N_4 and AuAg/g-C_3N_4 impregnated on the membranes

Fourier Transform Infrared Spectroscopy (FT-IR) was performed to confirm the presence of g-C_3N_4 in a Perkin-Elmer Two FT-IR equipment covering a range from 500 to 4000 cm^{-1}. A spatula was used to scrape off the material on the membrane surface in order to perform a FT-IR analysis. Excitation and emission spectra were recorded on a Shimadzu RF-6000 Spectrofluorophotometer (PL) with a solid accessory in which the membrane was placed. Diffuse reflectance UV–Vis (DRS) data of the membranes were recorded on a Shimadzu UV-3600 spectrophotometer with a Harrick Praying Mantis accessory by lowering the sample holder and placing the membrane on top. The diffuse reflectance spectra were obtained and recalculated applying the Kubelka-Munk function, leading to the solid-state absorption spectra. Scanning electron microscope (SEM) measurements were recorded on a Zeiss EVO 15 (operating at a 5–10 kV voltage) with detectors of cathodoluminescence and secondary and backscattered electrons. A sputter coating of gold-palladium was first applied onto the membrane in order to inhibit charging and improve secondary electron emission. Energy dispersive X-ray (EDX), used to analyse the chemical composition of the material, was registered on a SmartEDX (ZEISS).

2.5. Photocatalytic activity measurement

Firstly, tests were carried out under static conditions, i.e. membranes impregnated with photocatalyst were immersed in 20 mL of studied water inside a petri dish. Two prepared petri dishes were placed in the Equipment Photolab (LED365-1/450-1/850-1cb, Apria Systems, Spain). The first one was in dark conditions and the second one was irradiated with visible light (i.e. radiation = 1146 W/m^2), with exposure times of up to 6 h. Experiments with solar light, in static conditions, were performed on March 13, 2023 in Logroño (Spain), between 10:00 and 16:00 h, with mean radiation = 683 ± 108 W/m^2 [19]. RhB concentration (starting from 1 ppm) was quantified in a UV–visible spectrophotometer (Agilent 8453, Agilent Technologies, USA) at 554 nm (Fig. S1 - Supplementary material).

Dynamic experiments were conducted by placing the membranes in a filtration setup consisting of a glass funnel (15 mL capacity) with a base where the membrane was incorporated with an O-ring sealing, stopper, spring clamp and ground joint flask (Image S4 - Supplementary material). Gravity filtration was chosen firstly over vacuum filtration for the treatment in order to both reduce operating costs in decentralized systems and extend the reaction time. Filtration setup was placed under the visible lamp of the Photolab equipment (Image S4). Reading of the filtered volume and RhB concentration in both filtered and unfiltered water was performed after 6 h exposure time. If some of the studied water remained unfiltered past the 6-hour mark, it was vacuum filtered

Table 1
Membrane weight before and after g-C_3N_4 deposition.

Membrane n°	Pore size	IMF (g)	Mass melamine on top (g)	IMF + adhered g-C_3N_4 (g)	g-C_3N_4 deposited into membrane (g)	g-C_3N_4 into membrane (%)	IMF + adhered g-C_3N_4 (Mass after first use) (g)	g-C_3N_4 loss after first use (%)
2	40–100 μm	1.0586	1.0024	1.1816	0.123	10	1.1778	3.1
3	16–40 μm	0.8707	1.0004	1.0919	0.2212	20	1.0858	2.8
2-AuAg	40–100 μm	1.0747	1.0087	1.2254	0.1507	12	–	–
3-AuAg	16–40 μm	0.9113	1.006	1.1655	0.2542	22	–	–

Note: – not measured; IMF: initial mass of sintered glass filter (i.e. membrane).

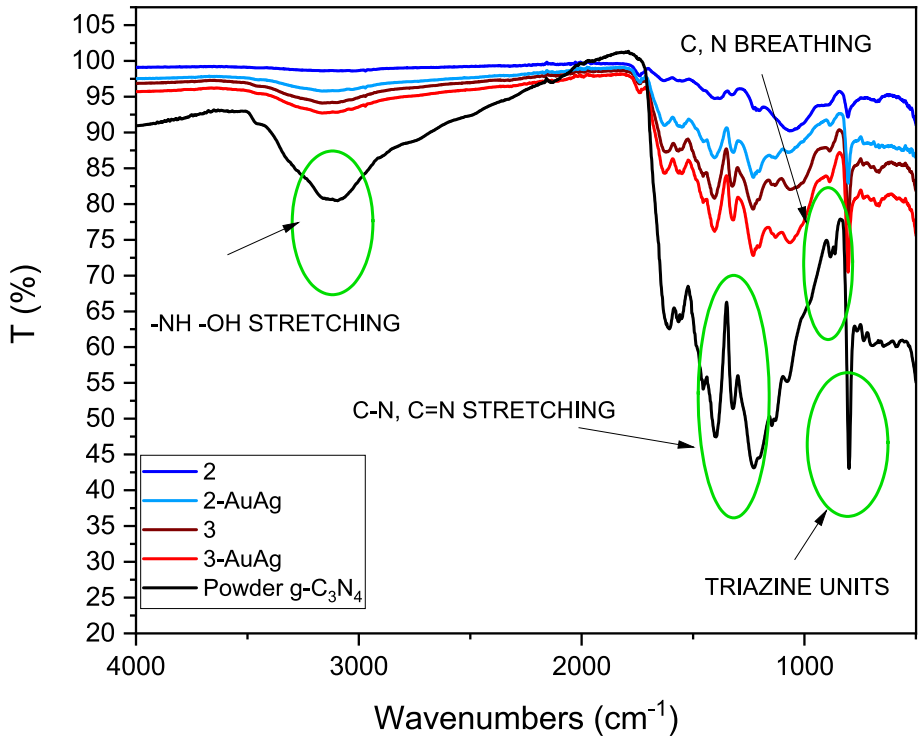

Fig. 1. FT-IR spectra of the samples with g-C_3N_4 deposited on membranes and the powder g-C_3N_4 sample (Notes: 2: membrane with porosity n° 2 with g-C_3N_4, 3: membrane with porosity n° 3 with g-C_3N_4; AuAg: membranes with NPs).

and the overall RhB concentration with the 15 mL filtered was recorded as well.

Studied water with turbidity was analysed in the filtration setup. First, the two membranes more susceptible to being affected by pore blockage (porosity 3) were subjected to 6 h trial (i.e. water with ~5 NTU and 1.0 ppm RhB). This test allowed us to verify if the turbidity was detrimental to the membrane or degradation capacity of the filtration setup. Studied water with turbidity was prepared by adding kaolin to ultra-pure water following the same procedure described in Jones and Bridgeman [20]. Studied water was subjected to a particle size distribution test in equipment Malvern (ZEN 3690). The mean size was found to be 2639 nm, with a minimum of 0.4 and a maximum of 10,000 nm and more proportion between 250 and 400 nm. 4 g of kaolin was added to 40 mL of ultra-pure water and the suspension was stirred for 30 min. The suspension was allowed to stand for 8 days, after which the supernatant was decanted and 0.3 mL was mixed with 1 L of ultra-pure water and, then, diluted x 10 to obtain studied water with turbidity ~5 NTU. It is highlighted that WHO [21] established that the turbidity of drinking water should not be >5 NTU. There was no adsorption between the kaolin and RhB, according to preliminary tests carried out.

2.6. Cost analysis

Two prototypes were designed in AutoCad 2020 (Autodesk, USA) with a light source using UV-LEDs or sun. The daily production was 500 L to supply up to five people. A per capita consumption of 100 L/person per day was considered to meet basic needs, as recommended by Ki-moon et al [22]. Initial investment was evaluated for Brazil and Spain including the main components (i.e.: tanks, pipes, fittings, valves, pump, metal structure, photocatalysis system, sintered glass membranes, chemicals for synthesis, electrical components, labour and control box), budgeted on 16 February 2024. Costs associated with operation, maintenance, transport, follow-up, taxes and indirect costs were not included in the economic evaluation.

2.7. Statistical analysis

Obtained data were analysed using statistical methods to determine significant differences (95 % confidence level, $p < 0.05$) among the datasets. First, normality distributions were assessed using the Shapiro-Wilk test, followed by the application of hypothesis tests. Given that all databases exhibited normal distributions, comparisons were made using

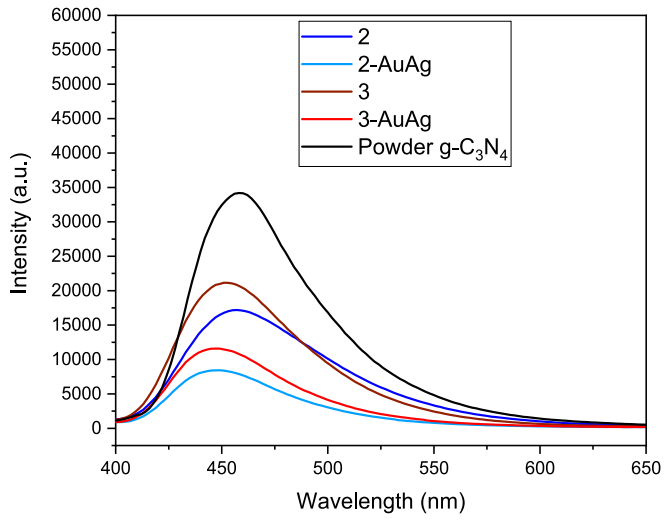

Fig. 2. Photoluminescent spectra for the samples with g-C_3N_4 deposited on membrane and powder g-C_3N_4 (Notes: 2: membrane with porosity n° 2 with g-C_3N_4, 3: membrane with porosity n° 3 with g-C_3N_4; AuAg: membranes with NPs).

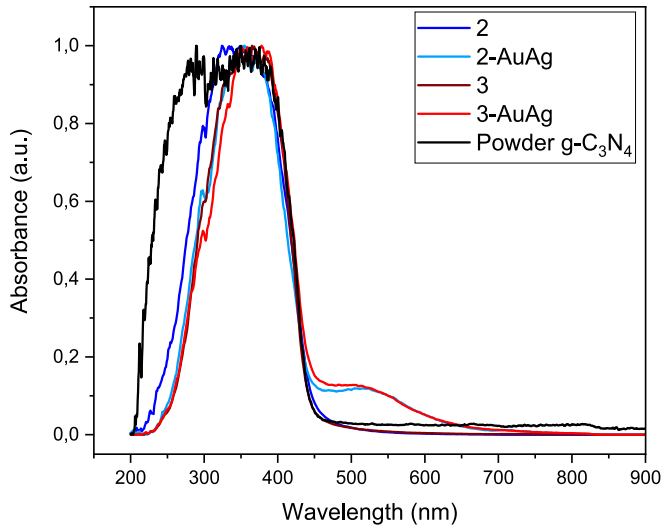

Fig. 3. Solid UV–Vis spectra (Notes: 2: membrane with porosity n° 2 with g-C_3N_4, 3: membrane with porosity n° 3 with g-C_3N_4; AuAg: membranes with NPs).

both the *t*-test and ANOVA several-sample test. Additionally, Spearman correlation was conducted to explore the relationship between the time of usage (quantified by the number of rounds) and the filtration volumes and rhodamine degradation capabilities. Significant correlation was defined when the *p*-value < 0.05 and the module of Spearman coefficient $|r|$ was greater than the module of r-critical. PAST software developed by Hammer et al [23] was used on all statistical analyses.

3. Results and discussion

3.1. Characterization g-C_3N_4 and AuAg/g-C_3N_4 impregnated into membranes

The amount of g-C_3N_4 deposited on the membranes was measured by weighing them before and after deposition (Table 1).

Membranes with porosity 2 had a higher initial mass, which was not translated into a bigger amount of g-C_3N_4 deposited on its surface. Due to the smoother surface of the membranes with porosity 3 as they have smaller pore size (Image S5 - Supplementary material), which is translated into a higher surface area, these had more g-C_3N_4 deposited on top. The loss of g-C_3N_4 after the first static test was around of 3 %.

The structure of the catalyst was assessed by FT-IR and the obtained spectra is in Fig. 1.

The presence of g-C_3N_4 was confirmed in the four membranes and followed the same pattern as the powder g-C_3N_4 sample. The broad band appearing from 3000 to 3500 cm^{-1} can correspond to both the –O–H of adsorbed H_2O and, more probably, the stretching vibration of N—H of the amino groups. From 1250 to 1700 cm^{-1}, the stretching vibrations of both C—N and C═N (inside/outside the triazine rings) appear [24] and the adsorption peak at 801 cm^{-1} is due to the ring structures in the layers of carbon nitride vibrating out of plane [25].

Photoluminescent properties (PL) analyses were also performed for the membranes and powder g-C_3N_4 (Fig. 2). A maximum at 460 nm was found in samples powder g-C_3N_4 and membrane 2 (excitation at ~363 nm) which is in the range generally obtained for this material [26], while in the rest of the samples was shifted to 450 nm. The greater intensity in porosity 3 membrane in relation to 2 could be would be related to a higher amount of C_3N_4 deposited on its surface, since its pores are smaller.

There are some limitations to the use of g-C_3N_4 for water remediation purposes that need to be overcome, mainly, its narrow window visible-light absorption and its high electron-hole recombination rate. An indirect evidence of the improvement of the photocatalyst can be seen when analysing its photoluminescent properties [27]. The emission band shown in Fig. 2 emerges when the photogenerated electron-hole pairs recombine in the interband. The effect that the direct deposition of the g-C_3N_4 into membrane has on the catalyst photoemissive properties can be readily seen, as the emission intensity is reduced in half. Both the Schottky barrier and the LSRP of the plasmonic AuAg NPs could be responsible for a further improvement of the electron-hole separation as the signal is yet reduced when the NPs are present in the samples, which may lead to improved photocatalytic properties [28].

The restricted margin of visible absorption characteristic of bulk g-C_3N_4 is expanded with the deposition of alloyed gold-silver nanoparticles on its surface. As can be seen in Fig. 3, the deposition of the g-C_3N_4 into membranes does not seem to modify its absorption capacity on the visible range.

The placement of the NPs on the surface of the sample has a similar effect on both samples, regardless the porosity of the membrane. The absorption peak of colloidal solutions of pure silver nanoparticles is situated at the higher energies (400–420 nm) and the absorption peak of pure gold (peak at ~520 nm) is situated at intermediate energy levels of the visible light [29]. The LSPR absorption of colloidal solutions of spherical alloyed AuAg NPs appears at intermediated wavelengths (460–480 nm). In solid state, the spherical AuAg NPs grafted on the g-C_3N_4 surface results in a stable and fairly intense absorption capacity from 450 to 550 nm, which then continues in a downward trend until well-passed 650 nm. Even though its absorption capacity seems to have no change when the g-C_3N_4 is deposited on the surface of the material, the band gap of the samples suffers from minor modifications. As can be seen in the Tauc plots in Fig. 4, the 2.77 eV initial band gap of powder g-C_3N_4 is slightly reduced when deposited on the membranes, obtaining 2.76 eV for sample 3 and 2.73 eV for sample 2.

The appearance of plasmonic absorption due to the nanoparticles leads to the same band gap to that of free g-C_3N_4, i.e. 2.77 eV for both porosities alike. This plasmonic absorption increases the visible light harvesting ability of both samples, also boosting the LSRP effects.

An approximate estimation of the band edge positions of the conduction band (CB) and the valence band (VB) for g-C_3N_4 can be calculated. The VB edge (E_{VB}) and the CB edge (E_{CB}) of a semiconductor at the point of zero charge can be calculated by the use of the following expressions [30–32]:

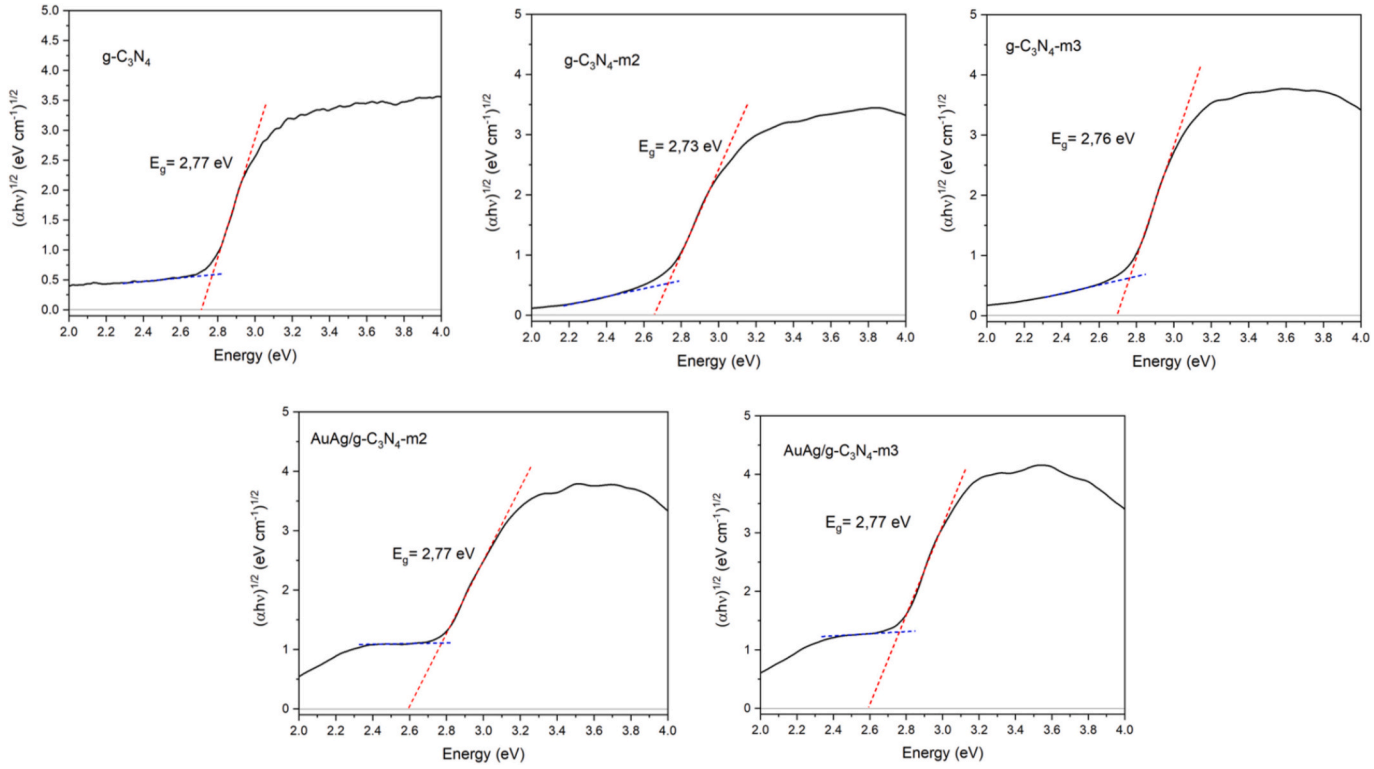

Fig. 4. Tauc plots for the g-C_3N_4 containing samples.

Table 2
Band gap energy of the semiconductor and calculated values for E_{VB} and E_{CB} for the different synthesized materials.

Sample	Band gap (eV)	E_{VB} (eV)	E_{CB} (eV)
g-C_3N_4-m2	2.73	1.595	−1.135
AuAg/g-C_3N_4-m2	2.76	1.610	−1.150
g-C_3N_4-m3	2.77	1.615	−1.155
AuAg/g-C_3N_4-m3	2.77	1.615	−1.155
g-C_3N_4	2.77	1.615	−1.155

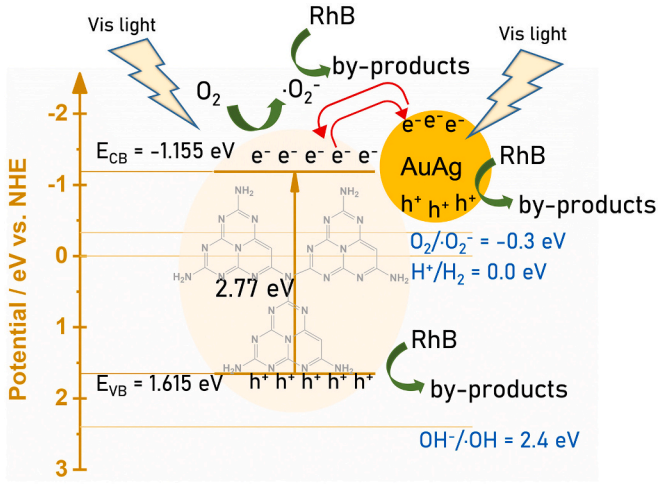

Scheme 1. Mechanism of reaction of the AuAg/g-C_3N_4-m3 catalyst.

$$E_{VB} = X \cdot E_e + 0.5E_g$$

$$E_{CB} = E_{VB} - E_g$$

where E_e is the energy of the free electrons (4.5 eV); E_g is the band gap energy of the semiconductor; and X is the absolute electronegativity of the semiconductor g-C_3N_4 (geometric mean of the absolute electronegativity of the atoms forming the semiconductor, 4.73 in the case of g-C_3N_4) [33].

Table 2 displays the calculated values for E_{VB} and E_{CB} for the different synthesized materials. The E_{VB} values range between 1.595 and 1.615 eV and the E_{CB} between −1.135 and 1.155 eV, depending on the membrane porosity and the presence or not of AuAg NPs grafted on g-C_3N_4 nanosheets. In any case, these values allow the design of an energy diagram of the photoexcited electron-hole separation processes for the explanation of the reaction mechanisms and the determination of the reactive oxygen species (see Scheme 1 below for sample AuAg/g-C_3N_4-m3).

The morphology of the sample with porosity 3 (after several uses) was analysed by scanning electron microscopy (SEM) and the micrographs obtained are shown in Fig. 5.

EDX analysis on the surface (Figs. S3 a S7 - Supplementary material) is useful to decipher the different structures present. The bigger and rounded particles corresponding to the borosilicate sintered glass membrane appear to be sitting on top. Borosilicate glass (containing silica, calcium and sodium carbonate) is manufactured with dehydrated borate, boric acid, alumina and sodium chloride. Percentage by weight of a typical analysis of borosilicate glass is in Table 3.

Analysis of a borosilicate glass at EDX4 (Fig. S6) confirms the presence of these elements, with nitrogen and boron missing, the latter due to interference at this low X-ray energy with other lightweight elements like oxygen. On the other hand, the mapping of a small surface containing only g-C_3N_4 (EDX5 Fig. S7) detects the presence of nitrogen (38 % atomic) and the signal of silicon is reduced from 35 to 5 %. The well-distributed laminar g-C_3N_4 can be observed throughout the sample,

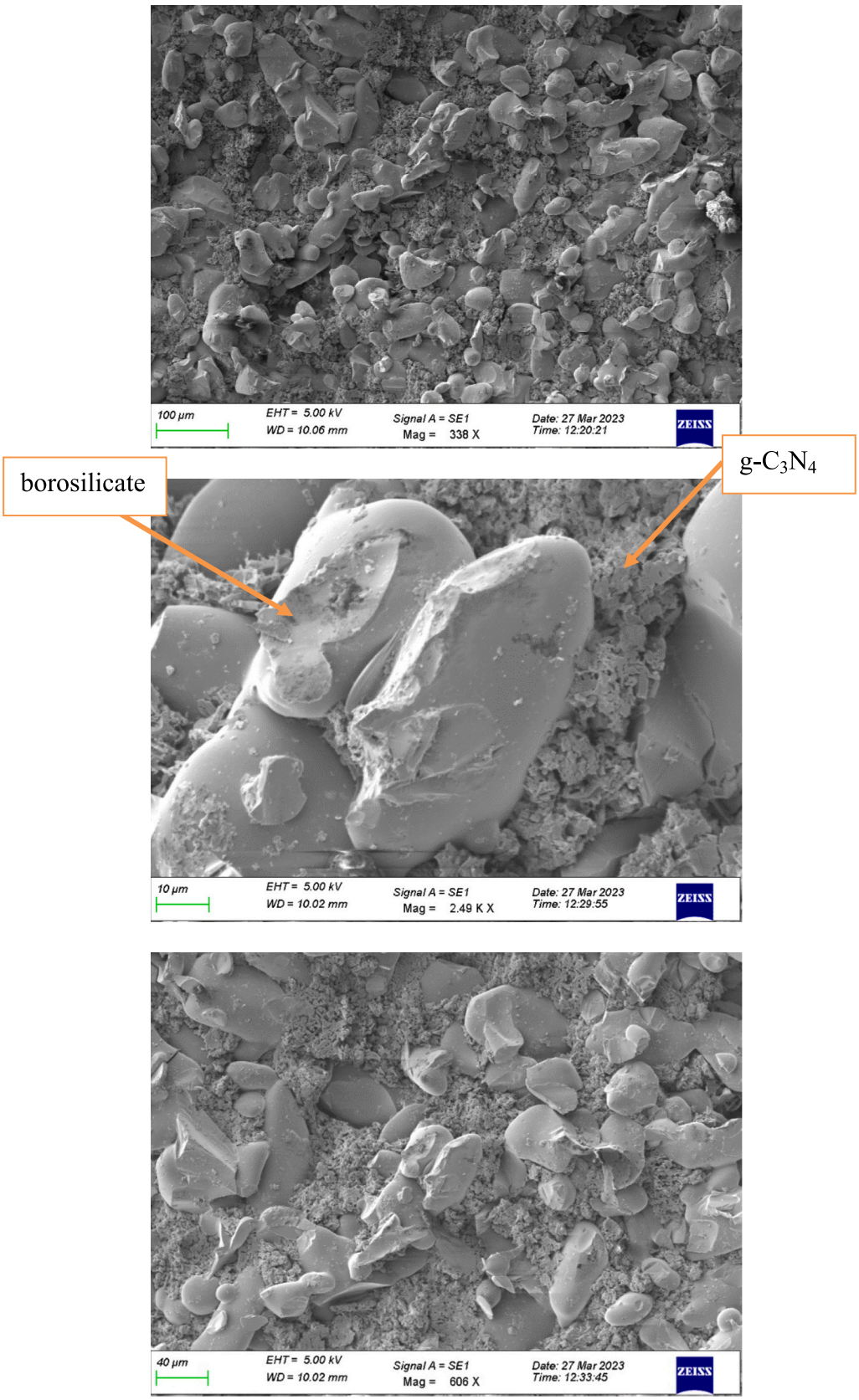

Fig. 5. SEM micrographs of the membrane with porosity 3 and g-C_3N_4 after several uses.

Table 3
Chemical composition of the borosilicate glass (element % by weight) (Robu glass, 2023) [34].

Element	%	Element	%
SiO_2	80.60	MgO	0.05
B_2O_3	12.60	Fe_2O_3	0.04
Na_2O	4.20	CaO	0.10
Al_2O_3	2.20	Cl	0.10

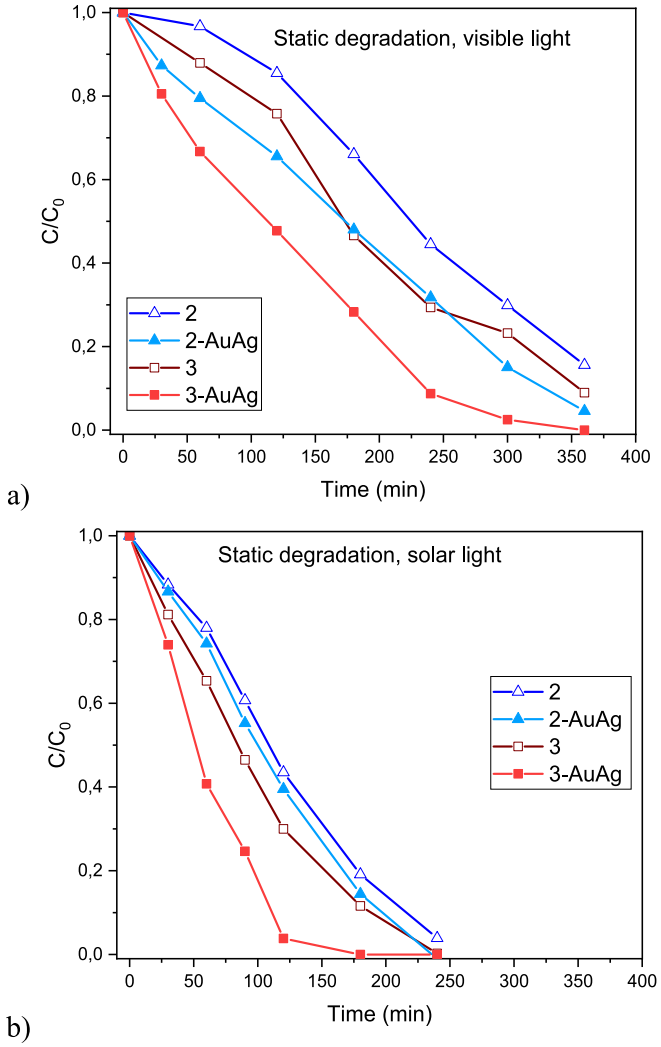

Fig. 6. Degradation results, under statics conditions, when under visible light (a) and solar light (b) (Notes: 2: membrane with porosity n° 2 with g-C_3N_4, 3: membrane with porosity n° 3 with g-C_3N_4; AuAg: membranes with NPs).

acting as filler that tries to balance out the surface. Its absence on the higher points of the particles may be due to the rubbing/washing carried out before or in-between uses. The surface of the membrane 2 would show a much uneven surface as its rougher appearance can be noticed with the naked eye (Image S5).

3.2. Photodegradation performance

3.2.1. Static studies

With the membranes placed inside the RhB solution, their performance under visible light and sunlight is displayed in Fig. 6.

Results in visible light and sunlight showed that membranes with porosity 3 degraded the target compound faster than porosity 2,

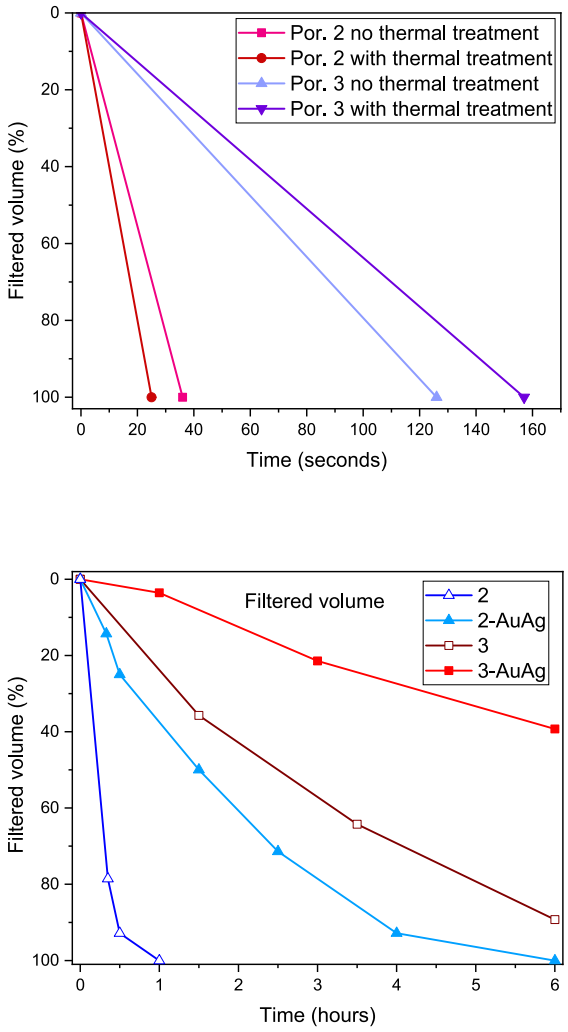

Fig. 7. Filtered volumes before and after thermal treatment (a) and filtered volumes after g-C_3N_4 and AuAg deposition (b) (Notes: 2: membrane with porosity n° 2 with g-C_3N_4, 3: membrane with porosity n° 3 with g-C_3N_4; AuAg: membranes with NPs).

probably because membrane 3 had more g-C_3N_4 impregnated, according to Table 1. The addition of AuAg-NPs improved the membrane performance for the tested porosities, reducing treatment time.

The use of sunlight decreased the degradation time from 6 h to 4 h (as approximately 6 % of solar light is UV radiation). The membrane 3 with AuAg reduced the RhB concentration to <4 % in just 2 h.

RhB degradation values were statistically correlated with time, that is, there was an increase in the degradation of the compound as a function of the increase in time. However, significant statistical differences were not found when analysing RhB degradation for membranes with porosities 2 and 3 with and without NPs (p-value > 0.05).

The proposed treatment managed to degrade >95 % of RhB, the change of colour of the aliquots extracted throughout the experiment is displayed as seen in Image S6 (Supplementary material). While the samples lose their characteristic pink colour under visible light (a), under UV light their orange fluorescence changes to green. This is due to the emission of the new fragments formed, as the aromatic ring present in RhB structure is eliminated.

Experiments performed in darkness for all the samples showed no adsorptions between membranes and RhB. Experiments done without catalyst (RhB under either UV or visible light) showed photolysis limited degradation capacity (12 % visible light, 0 % UV light), according to

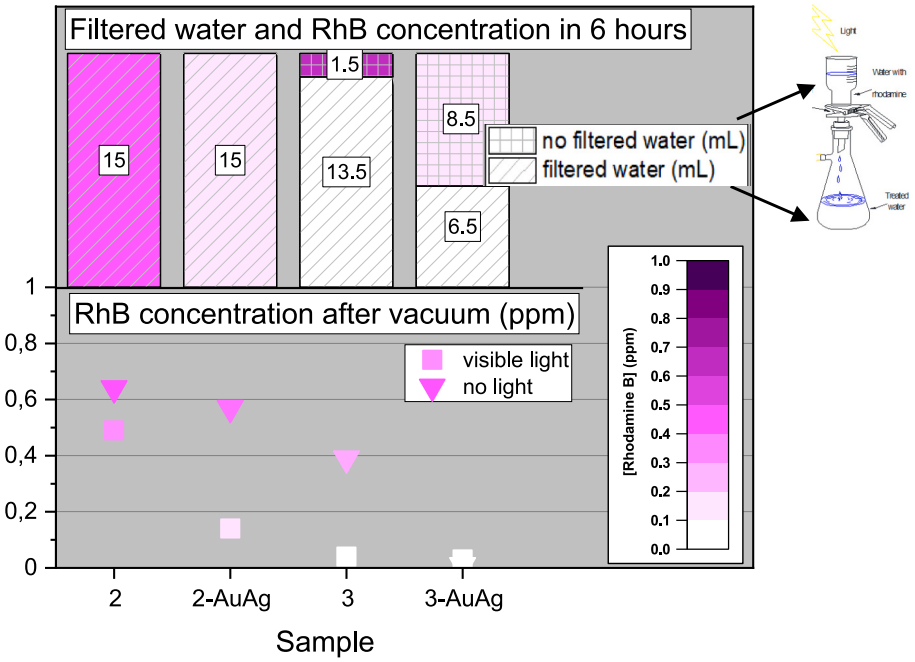

Fig. 8. RhB degradation and filtered volumes for each membrane (Notes: 2: membrane with porosity n° 2 with g-C_3N_4, 3: membrane with porosity n° 3 with g-C_3N_4; AuAg: membranes with NPs).

Table 4
Different membrane composition and synthesis methods for the photocatalytic removal of various pollutants reported in literature.

Method	Membrane composition	Degraded pollutant	Light	Photocatalytic capacity	Reference
Blending	Nano ZnO/cellulose acetate-polyureathane	Reactive red/orange dyes	UV light	–	[44]
Surface modification	Au-TiO_2 PDA-coated PVDF	Tetracycline	Visible light	92 %	[45]
Electrospun	PAN/g-C_3N_4/BiOI nanofibers	RhB Cr(VI)	Visible light	98 % 98.5 %	[46]
Vacuum filtration	RGO/PDA/g-C_3N_4/cellulose acetate	Methylene blue	Visible light	97.5 %	[47]
Liquid-based	metal free perylene imide/g-C_3N_4/SiO_2 with peroxymonosulfate	Bisphenol A	Visible light	100 %	[41]
Magnetically induced freezing casting method	Fe_3O_4/g-C_3N_4/PVDF	RhB	Visible light	97.8 %	[42]
Vapor deposition	Au-Ag NPs/g-C_3N_4/SiO_2	RhB	Visible light	100 %	This work

Notes: – not reported.

Fig. S2 (Supplementary material). A mechanism of the reaction-taking place between the catalyst and the pollutant has been proposed in Scheme 1.

When light hits the semiconductor, a photon with energy greater than its band gap forms an electron-hole pair (electrons moving from the valence band to the conduction band). When AuAg NPs are grafted to the catalyst, they act as electron traps of these electrons, thus improving the charge separation (as seen in PL results), disfavouring the electron-hole recombination. In addition, the LSPR effects can also help with the solar light harvesting of the catalyst, producing an additional charge carrier separation in the AuAg NPs, injecting the hot electrons in the conduction band of the semiconductor, precluding the fast electron-hole recombination in the bimetallic nanoparticles. From the different reactive oxygen species that can be generated, the combination of the holes (h^+) and superoxide radicals (O_2/$^\bullet O_2^-$) seem to be the most plausible. The CB edge of carbon nitride is more negative, being around −1.20 eV, (vs. NHE) than the O_2/$^\bullet O_2^-$ potential (−0.33 eV, vs. NHE), therefore they could be produced in the reaction. However, the potential of hydroxyl radicals is outside the VB edge and these radicals could be only secondarily generated [35,36].

Reported studies carried out with Au and C_3N_4 combine both h^+ and $^\bullet O_2^-$ as active species when degrading methylene blue and RhB [29,37]. Also, some studies using g-C_3N_4 on the degradation of ciprofloxacin showed that the only active species responsible for the degradation are holes [38], while when combining AuAg nanoparticles with N-doped carbon/TiO_2, $^\bullet O_2^-$ also appear [39]. Thus, the combination of h^+ and $^\bullet O_2^-$ as active species in this photoreaction seems likely.

A more detailed study could better elucidate the formation of radicals, the by-products formed and the degradation mechanism, however the objective of the work at this time was to verify the viability/efficiency and costs of the filters as a membrane.

3.2.2. *Dynamic studies*

Filtered volumes as a function of time were measured in the tested membranes. Membranes before the g-C_3N_4 vapor deposition were studied first. Two membranes (porosities 2 and 3) were subjected to a thermal treatment similar to that of the vapor deposition procedure (i.e. 2 h at 500 °C followed by 2 h at 520 °C) and were compared with two

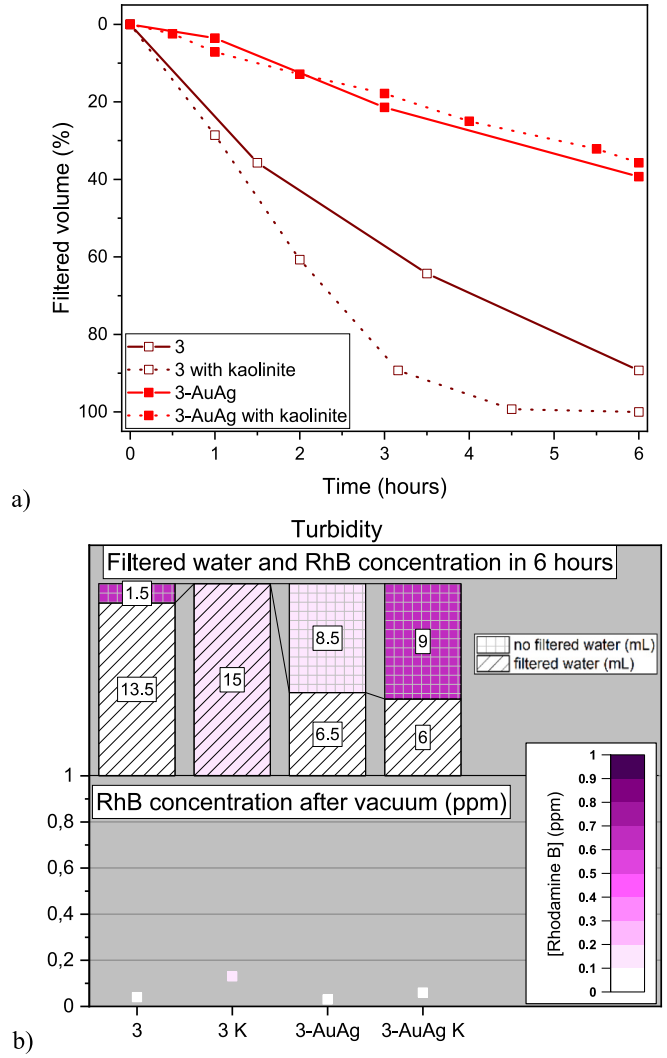

Fig. 9. (a) Filtered volumes for membrane 3 with and without turbidity, (b) RhB degradation and filtration capacity for membrane 3 with and without turbidity (Notes: 3: membrane with porosity n° 3 with g-C_3N_4; AuAg: membranes with NP, K: with kaolinite).

non-thematically treated membranes. The results are displayed in Fig. 7a.

Filtered volumes were quite fast for the 15 mL of studied water (t = ~30 s for porosity 2 with filtration rate = ~138 m^3/m^2d and t = ~140 s for porosity 3 with filtration rate = ~29 m^3/m^2d). The thermal treatment had no apparent effect on filtered volumes. The effect of heat treatment to incorporate g-C_3N_4 into the membrane was apparently not responsible for the low filtration rate, according to the manufacturer; these membranes have a deformation point at a temperature above 580 °C, which is above the 520 °C employed for the synthesis of the membranes. The impregnation of g-C_3N_4 in the membrane reduced the filtration rate since those without photocatalysts only needed a few seconds to filter the sample (Fig. 7a, b). The effect of the NPs was also studied and showed an effect in the filtration volume of the membranes. When analysing Fig. 7b, filtration rates were between 1.9 and 11.4 m^3/m^2 d. It is observed that membrane 2 was able to filter the 15 mL of sample in 1 h without NPs and in 6 h with them. On the other hand, part of the sample cannot be filtered by gravity on membranes of porosity 3, that is, in 6 h only 90 % of the sample was filtered on the membrane without NPs and only 40 % on the membrane with NPs. Tests with porosity 3 required vacuum filtration after 6 h of exposure time.

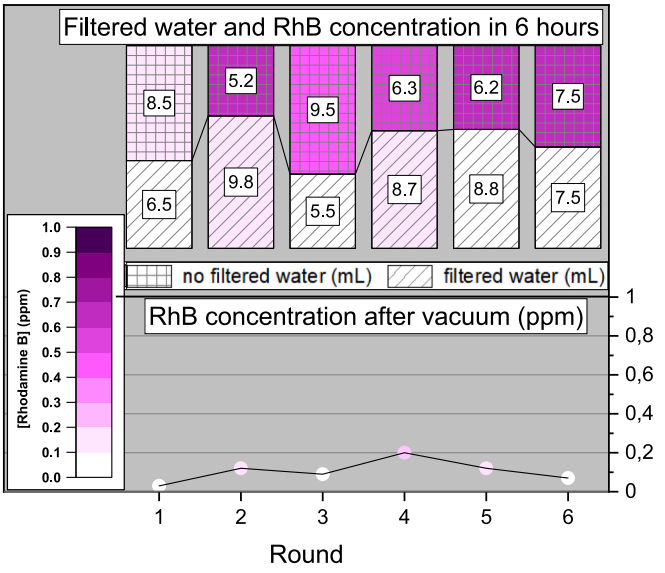

Fig. 10. Filtrated volume and RhB degradation for membrane 3-AuAg after 6 cycles.

3.2.3. *RhB degradation and filtered volumes*

Filtered volumes and RhB concentrations for each membrane are at the top of the Fig. 8. Membranes with porosity 2 can filtrate the 15 mL of water in 6 h without the need for a vacuum pump. Membrane 2 with AuAg works well due to both the degradation efficiency and the slower filtered volume, which leaves the studied water in contact with the filter/light for a longer time.

Membranes with porosity 3 are not able to filter all the studied water. Both membranes with and without NPs eliminate the target compound; in the case of 3-AuAg, 88 % of the non-filtered RhB is also degraded. The inferior part of Fig. 8 shows a comparison of RhB concentration of the 15 mL with visible light (■) or darkness (▼) after 6 h and vacuum needed for membrane 3. All membranes were capable of retaining some RhB without the need for light, membrane 3-AuAg retained all the RhB in the darkness filtering. The comparison of the RhB concentrations in the experiments with/without light show that there is not a big concentration difference for membrane 2 (36 vs 51 % removal) and membrane 3-AuAg (~100 % both visible and darkness). Membranes 2-AuAg and 3 better portray the effect of the light with degradation differences of 43 % and 35 %, respectively.

An interesting approach for obtaining both effective and larger filtered volumes in a short time would be the use of the 3-AuAg membrane with vacuum filtration, capable of retaining the RhB in dark conditions, and a posterior photocatalytic treatment of the filter, taking advantage of its faster self-cleaning capacity under visible or better, solar light.

Some studies have experimented positive results with the placement of g-C_3N_4 on different surfaces. Porous glass beads where selected by Hui et al. [40], where using a calcination method of coating g-C_3N_4 onto the beads its photocatalytic degradation of methyl orange was evaluated. Similar photocatalytic activity to P25 (TiO_2) coated glass beads in the removal of cyanobacterial toxins under UV light irradiation was observed. Other emerging pollutants, like Bisphenol A (BFA), were tested by Wang et al. [41] with metal free perylene imide-carbon nitride membranes synthesized via a liquid-based preparation method. Likewise, Li et al. [42] tested PVDF membranes with Fe_3O_4/g-C_3N_4 for the removal of RhB (300 W Xe lamp, $\lambda \geq 420$ nm) with a magnetically induced freezing casting method in order to distribute and embed the photocatalysts. Finally, Al_2O_3 substrate was coated with P-doped g-C_3N_4, which worked with visible light for the removal of methylene blue, methyl orange and phenol solution, showing high photocatalytic

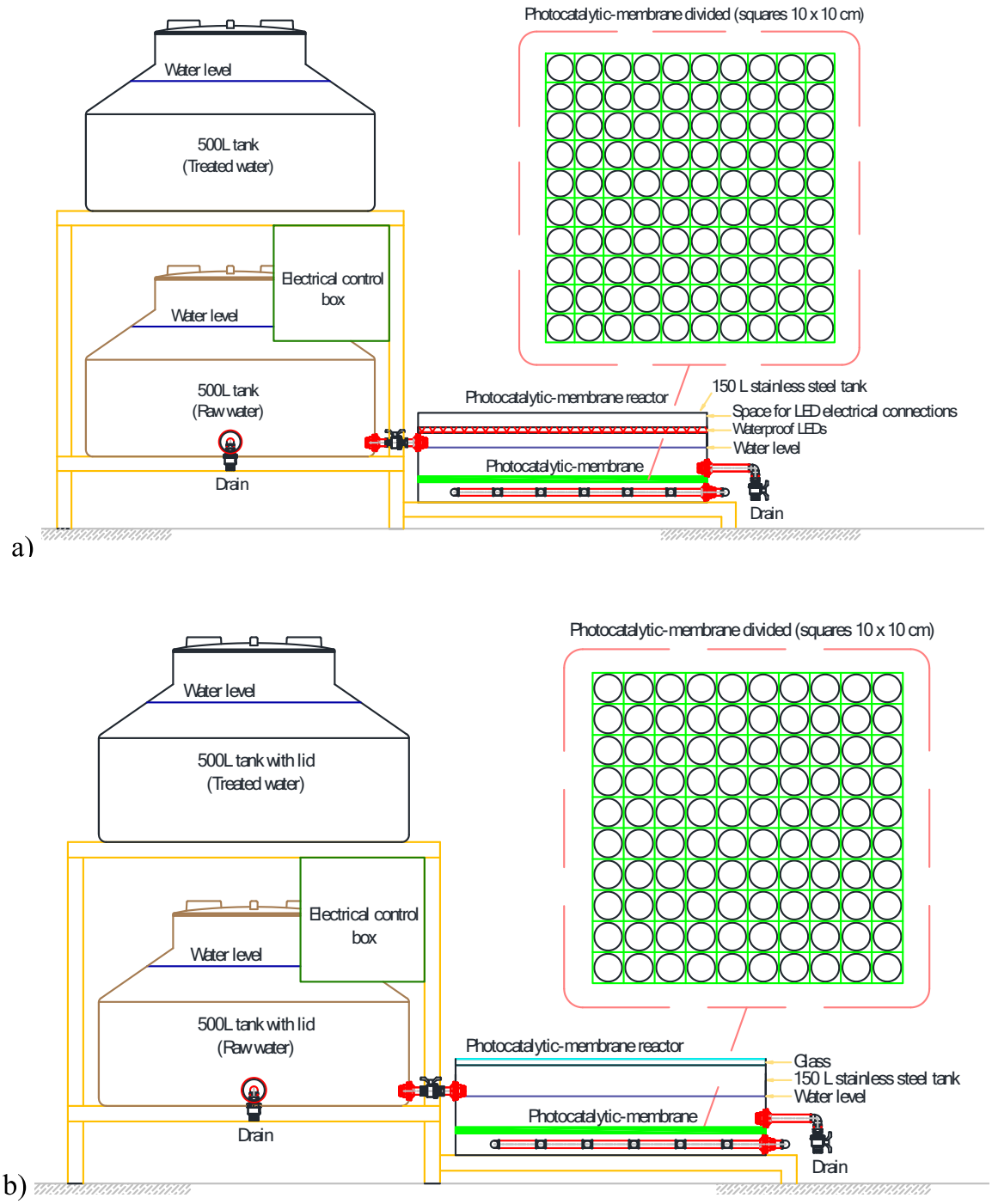

Fig. 11. Basic prototype of the photocatalyst-membrane reactor with dimensions of 1.0 m × 1.0 m for reactions that require >3 h of exposure time, a) light source: LEDs and b) light source: sun.

activity [43]. Table 4 showcases various effective methods of membrane synthesis reported in literature, when working with visible light, most of them use carbon nitride in their composition.

In order to compare our photocatalytic system with other hybrid nanomaterials in the degradation of dyes we can cite some previous results. For instance, Lee et al. reported on the degradation of RhB by using TiO_2 and gold nanoparticles supported on a floating porous polydimethylsiloxane sponge under ultraviolet and visible light irradiation, achieving 90 % of degradation of a 20 μM solution of RhB in 90 min [48]. In another study, Singh et al. showed that hybrid Ag nanoparticles supported on graphene photocatalyzes a 10 ppm solution of RhB up to 95 % of efficiency in 120 min by using a 300 W UV lamp [49]. The same group developed a RuO2/SWCNT nanocomposite that photocatalyzed the degradation of 10 ppm solution of Methylene Blue (MB) up to 95 % of efficiency in 100 min using a 300 W UV-lamp [50]. Our heterogenized AuAg/g-C_3N_4 photocatalyst eliminates 100 % of a 1 ppm solution of RhB by using a low-power visible light LED, what makes our system competitive for photocatalytic degradation of pollutants in wastewaters.

3.2.4. *Turbidity effect*

Membranes with porosity 3 with and without NPs were subjected to experiments with turbid water (Fig. 9). The addition of kaolinite in the studied water did not cause significant effects on filtration capacity with g-C_3N_4 (p = 0.5635, t-test) and g-C_3N_4-Au/Ag (p = 0.9515, t-test).

Table 5
Initial investment of the photocatalyst-membrane reactor.

Photocatalytic-membrane reactor (1.0 m × 1.0 m) with LED light				
Item	Only with g-C_3N_4		g-C_3N_4 + Ag/Au	
	Cost (US$) Spain	Cost (US $) Brazil	Cost (US $) Spain	Cost (US $) Brazil
Basic infrastructure without photocatalytic-membrane reactor (i.e. tanks, pipes, fittings, valves, pump, metal structure, electrical components, labour and control box)	2622	1450	2622	1450
Photocatalytic-membrane reactor (1.0 m × 1.0 m) without g-C_3N_4 or Ag/Au (i.e. photocatalysis system and sintered glass membranes)	3594	2808	3594	2808
Membrane impregnated with g-C_3N_4 only (i.e. chemicals for synthesis and energy consumption)	321	745	–	–
Membrane impregnated with g-C_3N_4 + Ag/Au (i.e. chemicals for synthesis and energy consumption)	–	–	14,873	10,511
Total	6537	5004	21,088	14,770

Photocatalytic-membrane reactor (1.0 m × 1.0 m) with sunlight				
Item	Only with g-C_3N_4		g-C_3N_4 + Ag/Au	
	Cost (US$) Spain	Cost (US $) Brazil	Cost (US $) Spain	Cost (US $) Brazil
Basic infrastructure without Photocatalytic-membrane reactor (i.e. tanks, pipes, fittings, valves, pump, metal structure, electrical components, labour and control box)	2622	1450	2622	1450
Photocatalytic-membrane reactor (1.0 m × 1.0 m) without g-C_3N_4 or AuAg (i.e. photocatalysis system and sintered glass membranes)	2353	1913	2353	1913
Membrane impregnated with g-C_3N_4 only (i.e. chemicals for synthesis and energy consumption)	321	745	–	–
Membrane impregnated with g-C_3N_4 + Ag/Au (i.e. chemicals for synthesis and energy consumption)	–	–	14,873	10,511
Total	5296	4109	19,848	13,875

Note: Costs calculated on February 16, 2024, –: not applicable.

Nonetheless, the addition of NPs associated with the addition of kaolinite caused significant effects on the volume of filtered water. That is, in the treatment there was a significant effect of the insertion of NPs in the filtered volumes ($p = 0.011$, *t*-test). For water treatment without the addition of kaolinite, no effect of the addition of NPs on the volumes of filtered water was observed ($p = 0.191$, *t*-test). RhB degradation capacity of both samples is slightly reduced when kaolinite is added to the water (Fig. 9b). A slight increase in the RhB concentration is observed when all the water has been filtered by vacuum pump.

Even though the study of the catalyst performance in turbid water is essential for practical applications, there are not many studies that analyse the effect of turbidity on the degradation capacity of photocatalysts towards RhB. Persico et al. [51] studied that the presence of $BaSO_4$ microparticles (8 g/L, average particle dimension = 10 μm) reduced the degradation kinetic constant by a 40 %. In general, the effect of turbidity is mentioned in the catalyst dose, as for quantities over the best-performing dose, the light passage is hindered and the light scattering increased [52,53].

3.2.5. Stability test and degradation cycles

According to Fig. 8a, tests with membrane 3-AuAg showed a lower filtration capacity and an increased RhB degradation capacity than tests with membrane 3 and this result justified the choice of membrane 3-AuAg for the next phase of testing (i.e. 6 consecutive rounds). Once one round was finished, the glass funnel was filled again with 15 mL of the RhB solution with no cleaning/washing in-between. The results (see Fig. 10) indicated that filtrated volume does not show significant changes over time ($p = 0.758$, $|r| = 0.143$, $r_{critical} = 0.886$). In the same way, RhB degradation capacity did not substantially decrease over time ($p = 0.506$, $|r| = 0.348$, $r_{critical} = 0.886$) and there were no statistical differences when analysing the degradation capacity of the target compound after the 6 rounds ($p = 0.081$ $|r| = 0.771$, $r_{critical} = 0.886$). Other authors have similar results, with no obvious decrease in photocatalytic activity during reuse [45,46], although some membranes need a wash step in-between cycle [41,42,45]. These results suggest the potential to develop a photocatalyst-membrane reactor, which has both stability and efficiency.

3.2.6. Cost analysis

The prototypes created are shown in Fig. 11 with a photocatalyst-membrane area of 1.0 m × 1.0 m (details in Figs. S8 and S9). The calculated initial investment is in Table 5.

Regarding the economic analysis, the cost of 1.0 cm^2 of g-C_3N_4 impregnation on sintered glass filter as membrane was US$ 0.05 for Spain and US$ 0.02 for Brazil. When adding AuAg nanoparticles, the value increased considerably, as 1.0 cm^2 of AuAg/gC_3N_4 conjugation generated a cost of US$ 2.34 in Spain and US$ 1.65 in Brazil. In other words, the addition of NPs to the g-C_3N_4 increases the cost between 46 and 82 times.

Initial investment for the basic infrastructure for a drinking water treatment system with production of 500 L/day was US$ 2622 in Spain and US$ 1450 in Brazil (Table 5). The cost obtained in Brazil was similar to those estimated by Maciel et al [54] for a drinking water treatment system with production of 180 L/day.

Initial investment for the photocatalytic-membrane reactor with LEDs and sintered glass membrane (i.e. without g-C_3N_4 or AuAg/g-C_3N_4 impregnation) was US$ 3594 in Spain and US$ 2808 in Brazil. When adding g-C_3N_4 to the membrane, the cost increased US$ 321 in Spain and US$ 745 in Brazil; however, when adding nanoparticles AuAg, the membrane value rose between 14- and 46-times reaching values of US$ 14,873 and US$ 10,511 in the nations studied. When sunlight is used, the aforementioned values were reduced in the range of 6 to 23 % for both countries, according to the treatment configuration.

With LED light or sunlight, the proposed system has a high cost depending on the configuration adopted (i.e. between US$ 4109 to US$ 21,088, according to Table 5). The advantage of using solar light is that the initial investment was lower and electricity savings can be obtained in the everyday use. The results show that the initial investment depends on the cm^2 of membrane impregnated with the photocatalyst, which is a function of the compound to be degraded and the need or not for nanoparticles. In all evidence, the technology is still economically unviable as a decentralized treatment.

It is noteworthy that in recent years, there has been a considerable increase in research related to photocatalysis for water treatment; however, there is still no commercial system available on the market (Tugaoen et al. [55]). Key aspects such as high treatment costs, membrane clogging, release of the impregnated photocatalyst throughout the operating cycles and cleaning alternatives must be better analysed to make the technology viable on a full scale.

4. Conclusions

This study successfully reports for the first time the synthesis of sintered glass filter as membrane impregnated with g-C_3N_4 via a simple vapor deposition method and the effect of AuAg nanoparticles impregnated on its surface to degrade Rhodamine B. The deposition of g-C_3N_4 was confirmed by FT-IR and the effect that the AuAg nanoparticles had on both reducing the electron-hole recombination and increasing the absorption capacity on the visible range was verified by PL and DRS. Experiments in static conditions under visible light and sunlight showed that membranes with porosity 3 degraded the target compound faster than porosity 2, as they had more g-C_3N_4 impregnated. The addition of AuAg-NPs improved the membrane performance for the tested porosities, reducing treatment time. In dynamic conditions, RhB degradation capacity of both membranes was slightly reduced when kaolinite was added to water. Filtrated volume does not show significant changes over time, RhB degradation capacity did not substantially decrease over time and there were no statistical differences when analysing the degradation capacity of the target compound after the six rounds, highlighting the potential to develop a photocatalyst-membrane reactor, which has both stability and efficiency. However, economic sustainability of a photocatalyst-membrane reactor in decentralized areas will require more research, as the high costs involved currently impede its use in these contexts.

CRediT authorship contribution statement

Leticia Santamaría: Writing – original draft, Investigation, Formal analysis, Data curation. **Lyda Patricia Sabogal-Paz:** Writing – review & editing, Formal analysis, Data curation, Conceptualization. **Bárbara Luíza Souza Freitas:** Writing – review & editing. **Maria Teresa Hoffmann:** Writing – review & editing. **David Royo-Pareja:** Investigation. **José M. López-de-Luzuriaga:** Writing – review & editing, Supervision, Resources, Funding acquisition. **Miguel Monge:** Writing – review & editing, Supervision, Methodology, Funding acquisition, Conceptualization.

Declaration of competing interest

The authors declare that they have no known competing financial interests or personal relationships that could have appeared to influence the work reported in this paper.

Acknowledgements

The São Paulo Research Foundation – FAPESP (Process n ° 2022/12258-1) and National Council for Scientific and Technological Development – CNPq (processes n° 308070/2021-6 and 442074/2023-9) supported this work. J. M. L. L. and M.M. thank the DGI MICINN/FEDER (project number PID2022-139739NB-I00 (AEI/FEDER, UE)) and by "ERDF A way of making Europe" and the ADER–UR project 2023-I-IDD-00019. L.S. thanks the Universidad Pública de Navarra for a post-doctoral Margarita Salas grant, financed by the European Union-Next Generation EU.

Appendix A. Supplementary data

Supplementary data to this article can be found online at https://doi.org/10.1016/j.jwpe.2024.106300.

Data availability

No data was used for the research described in the article.

References

[1] D. Zhang, R.M. Gersberg, C. Wilhelm, M. Voigt, Decentralized water management: rainwater harvesting and greywater reuse in an urban area of Beijing, China, Urban Water J. 6 (2009) 375–385, https://doi.org/10.1080/15730620902934827.
[2] Y. Kang, Y. Yang, L.C. Yin, X. Kang, G. Liu, H.M. Cheng, An amorphous carbon nitride photocatalyst with greatly extended visible-light-responsive range for photocatalytic hydrogen generation, Adv. Mater. 27 (2015) 4572–4577, https://doi.org/10.1002/adma.201501939.
[3] W.-J. Ong, L.-L. Tan, Y.H. Ng, S.-T. Yong, S.-P. Chai, Graphitic carbon nitride (g-C_3N_4)-based photocatalysts for artificial photosynthesis and environmental remediation: are we a step closer to achieving sustainability? Chem. Rev. 116 (2016) 7159–7329, https://doi.org/10.1021/acs.chemrev.6b00075.
[4] J. Wen, J. Xie, X. Chen, X. Li, A review on g-C_3N_4 -based photocatalysts, Appl. Surf. Sci. 391 (2017) 72–123, https://doi.org/10.1016/j.apsusc.2016.07.030.
[5] X. Liu, R. Ma, L. Zhuang, B. Hu, J. Chen, X. Liu, X. Wang, Recent developments of doped g-C_3N_4 photocatalysts for the degradation of organic pollutants, Crit. Rev. Environ. Sci. Technol. 51 (2021) 751–790, https://doi.org/10.1080/10643389.2020.1734433.
[6] L.M. Liz-Marzán, Tailoring surface plasmons through the morphology and assembly of metal nanoparticles, Langmuir 22 (2006) 32–41, https://doi.org/10.1021/la0513353.
[7] R. Kavitha, P.M. Nithya, S. Girish Kumar, Noble metal deposited graphitic carbon nitride based heterojunction photocatalysts, Appl. Surf. Sci. 508 (2020) 145142, https://doi.org/10.1016/j.apsusc.2019.145142.
[8] K.L. Kelly, E. Coronado, L.L. Zhao, G.C. Schatz, The optical properties of metal nanoparticles: the influence of size, shape, and dielectric environment, J. Phys. Chem. B 107 (2003) 668–677, https://doi.org/10.1021/jp026731y.
[9] C.-H. Chou, F.-C. Chen, Plasmonic nanostructures for light trapping in organic photovoltaic devices, Nanoscale 6 (2014) 8444–8458, https://doi.org/10.1039/C4NR02191F.
[10] X. Li, J. Zhu, B. Wei, Hybrid nanostructures of metal/two-dimensional nanomaterials for plasmon-enhanced applications, Chem. Soc. Rev. 45 (2016) 3145–3187, https://doi.org/10.1039/C6CS00195E.
[11] M. Volokh, T. Mokari, Metal/semiconductor interfaces in nanoscale objects: synthesis, emerging properties and applications of hybrid nanostructures, Nanoscale Adv. 2 (2020) 930–961, https://doi.org/10.1039/C9NA00729F.
[12] M.R. Khan, T.W. Chuan, A. Yousuf, M.N.K. Chowdhury, C.K. Cheng, Schottky barrier and surface plasmonic resonance phenomena towards the photocatalytic reaction: study of their mechanisms to enhance photocatalytic activity, Catal. Sci. Technol. 5 (2015) 2522–2531, https://doi.org/10.1039/C4CY01545B.
[13] J. Fu, J. Yu, C. Jiang, B. Cheng, g-C_3N_4-based heterostructured photocatalysts, Adv. Energy Mater. 8 (2018) 1–31, https://doi.org/10.1002/aenm.201701503.
[14] A. Müller, S.C. Weiss, W. Schulz, W. Seitz, R. Albert, W.K.L. Ruck, W.H. Weber, Combination of different liquid chromatography/mass spectrometry technologies for the identification of transformation products of rhodamine B in groundwater, Rapid Commun. Mass Spectrom. 24 (2010) 659–666, https://doi.org/10.1002/rcm.4430.
[15] L.M. Skjolding, L.v.G. Jørgensen, K.S. Dyhr, C.J. Köppl, U.S. McKnight, P. Bauer-Gottwein, P. Mayer, P.L. Bjerg, A. Baun, Assessing the aquatic toxicity and environmental safety of tracer compounds Rhodamine B and Rhodamine WT, Water Res. 197 (2021) 117109, https://doi.org/10.1016/j.watres.2021.117109.
[16] R. Usón, A. Laguna, J. Vicente, Preparation and properties of stable salts containing mono- or bis-(pentafluorophenyl)aurate(I) and mono-, tris-, or tetrakis-(pentafluorophenyl)aurate(III) ions, J. Chem. Soc. Chem. Commun. (1976) 353–354, https://doi.org/10.1039/C39760000353.
[17] R. Usón, A. Laguna, M. Laguna, B.R. Manzano, P.G. Jones, G.M. Sheldrick, Synthesis and reactivity of bimetallic Au–Ag polyfluorophenyl complexes; crystal and molecular structures of [{AuAg(C_6F_5)$_2$(SC_4H_8)}] and [{AuAg(C_6F_5)$_2$(C_6H_6)}], J. Chem. Soc. Dalton Trans. (1984) 285–292, https://doi.org/10.1039/DT9840000285.
[18] R. Uson, A. Laguna, M. Laguna, D.A. Briggs, H.H. Murray, J.P. Fackler Jr., (Tetrahydrothiophene)gold(I) or gold(III) complexes, in: Inorg. Synth, John Wiley & Sons, Ltd, 1989, pp. 85–91, https://doi.org/10.1002/9780470132579.ch17.
[19] Logroño meteorological station data. https://www.larioja.org/emergencias-112/es/meteorologia/datos-actuales-rioja/detalle-estacion?homepage=9&cod_muni=89, 2023.
[20] A.N. Jones, J. Bridgeman, Investigating the characteristic strength of flocs formed from crude and purified Hibiscus extracts in water treatment, Water Res. 103 (2016) 21–29, https://doi.org/10.1016/j.watres.2016.07.019.
[21] World Health Organization, Guidelines for Drinking-Water Quality, 4th edition, Incorporating the 1st Addendum, 2017, https://doi.org/10.5005/jp/books/11431_8.
[22] B. Ki-moon, The Human Right to Water and Sanitation Media Brief, 2010.
[23] Ø. Hammer, D.A.T. Harper, P.D. Ryan, Past: paleontological statistics software package for education and data analysis, Palaeontol. Electron. 4 (2001) 9.
[24] L. Luo, A. Zhang, M.J. Janik, C. Song, X. Guo, Facile fabrication of metal-free urchin-like g-C_3N_4 with superior photocatalytic activity, RSC Adv. 6 (2016) 94496–94501, https://doi.org/10.1039/c6ra20940h.
[25] S. Li, Y. Peng, C. Hu, Z. Chen, Self-assembled synthesis of benzene-ring-grafted g-C_3N_4 nanotubes for enhanced photocatalytic H2 evolution, Appl. Catal. B Environ. 279 (2020) 119401, https://doi.org/10.1016/j.apcatb.2020.119401.
[26] M. Jiménez-Salcedo, M. Monge, M.T. Tena, Combination of Au-Ag plasmonic nanoparticles of varied compositions with carbon nitride for enhanced photocatalytic degradation of ibuprofen under visible light, Materials (Basel) 14 (2021), https://doi.org/10.3390/ma14143912.

[27] J. Huang, S. Liu, W. Long, Q. Wang, X. Yu, S. Li, Highly enhanced photodegradation of emerging pollutants by Ag/AgCl/Ta_2O_{5-x} mesocrystals, Sep. Purif. Technol. 279 (2021) 119733, https://doi.org/10.1016/j.seppur.2021.119733.
[28] E. Alwin, R. Wojcieszak, K. Kočí, M. Edelmannová, M. Zieliński, A. Suchora, T. Pędziński, M. Pietrowski, Reductive modification of carbon nitride structure by metals—the influence on structure and photocatalytic hydrogen evolution, Materials (Basel) 15 (2022), https://doi.org/10.3390/ma15030710.
[29] S. Tonda, S. Kumar, V. Shanker, Surface plasmon resonance-induced photocatalysis by Au nanoparticles decorated mesoporous g-C_3N_4 nanosheets under direct sunlight irradiation, Mater. Res. Bull. 75 (2016) 51–58, https://doi.org/10.1016/j.materresbull.2015.11.011.
[30] B. Choudhury, A. Choudhury, Lattice distortion and corresponding changes in optical properties of CeO2 nanoparticles on Nd doping, Curr. Appl. Phys. 13 (2013) 217, https://doi.org/10.1016/j.cap.2012.07.014.
[31] N.S. Arul, D. Mangalaraj, R. Ramachandran, A.N. Grace, J.I. Hana, Fabrication of CeO_2/Fe_2O_3 composite nanospindles for enhanced visible light driven photocatalyst and supercapacitor electrode, J. Mater. Chem. A 3 (2015) 15248–15258, https://doi.org/10.1039/C5TA02630J.
[32] A. Kumar, S.K. Trivedi, L. Phor, J. Malik, S. Bhargava, V. Kaushik, P. Kumar, S. Chahal, Visible light activated Mg, Co co-doped hematite for effective removal of reactive red 35 from textile wastewater, Ceram. Int. 49 (2023) 37691–37699, https://doi.org/10.1016/j.ceramint.2023.09.095.
[33] M. Jiménez-Salcedo, M. Monge, M.T. Tena, The photocatalytic degradation of sodium diclofenac in different water matrices using g-C_3N_4 nanosheets: a study of the intermediate by-products and mechanism, J. Environ. Chem. Eng. 9 (2021) 105827, https://doi.org/10.1016/J.JECE.2021.105827.
[34] Robu glass. https://www.robuglas.com/fileadmin/dateien/Bilder/Service/Downloads/Technische_Daten_im_Detail_eng/datasheet_vitrapor_e.pdf, 2023.
[35] S. Chen, Y. Hu, S. Meng, X. Fu, Study on the separation mechanisms of photogenerated electrons and holes for composite photocatalysts g-C_3N_4-WO_3, Appl. Catal. B Environ. 150–151 (2014) 564–573, https://doi.org/10.1016/j.apcatb.2013.12.053.
[36] W. Zhang, L. Zhou, J. Shi, H. Deng, Fabrication of novel visible-light-driven AgI/g-C_3N_4 composites with enhanced visible-light photocatalytic activity for diclofenac degradation, J. Colloid Interface Sci. 496 (2017) 167–176, https://doi.org/10.1016/j.jcis.2017.02.022.
[37] M. Faisal, M. Jalalah, F.A. Harraz, A.M. El-Toni, A. Khan, M.S. Al-Assiri, Au nanoparticles-doped g-C_3N_4 nanocomposites for enhanced photocatalytic performance under visible light illumination, Ceram. Int. 46 (2020) 22090–22101, https://doi.org/10.1016/j.ceramint.2020.05.250.
[38] M. Jiménez-Salcedo, M. Monge, M.T. Tena, Study of intermediate by-products and mechanism of the photocatalytic degradation of ciprofloxacin in water using graphitized carbon nitride nanosheets, Chemosphere 247 (2020), https://doi.org/10.1016/j.chemosphere.2020.125910.
[39] M. Jiménez-Salcedo, M. Monge, M.T. Tena, AuAg nanoparticles grafted on TiO_2@N-doped porous carbon: improved depletion of ciprofloxacin under visible light through plasmonic photocatalysis, Nanomaterials 12 (2022), https://doi.org/10.3390/nano12152524.
[40] J. Hui, C.J. Pestana, M. Caux, H.Q.N. Gunaratne, C. Edwards, P.K.J. Robertson, L. A. Lawton, J.T.S. Irvine, Graphitic-C_3N_4 coated floating glass beads for photocatalytic destruction of synthetic and natural organic compounds in water under UV light, J. Photochem. Photobiol. A Chem. 405 (2021) 112935, https://doi.org/10.1016/j.jphotochem.2020.112935.
[41] Y. Wang, H. Wang, J. Li, X. Zhao, Facile synthesis of metal free perylene imide-carbon nitride membranes for efficient photocatalytic degradation of organic pollutants in the presence of peroxymonosulfate, Appl. Catal. B Environ. 278 (2020) 118981, https://doi.org/10.1016/j.apcatb.2020.118981.
[42] B. Li, M. Meng, Y. Cui, Y. Wu, Y. Zhang, H. Dong, Z. Zhu, Y. Feng, C. Wu, Changing conventional blending photocatalytic membranes (BPMs): focus on improving photocatalytic performance of Fe3O4/g-C3N4/PVDF membranes through magnetically induced freezing casting method, Chem. Eng. J. 365 (2019) 405–414, https://doi.org/10.1016/j.cej.2019.02.042.
[43] C. Hu, M.S. Wang, C.H. Chen, Y.R. Chen, P.H. Huang, K.L. Tung, Phosphorus-doped g-C_3N_4 integrated photocatalytic membrane reactor for wastewater treatment, J. Membr. Sci. 580 (2019) 1–11, https://doi.org/10.1016/j.memsci.2019.03.012.
[44] A. Rajeswari, S. Vismaiya, A. Pius, Preparation, characterization of nano ZnO-blended cellulose acetate-polyurethane membrane for photocatalytic degradation of dyes from water, Chem. Eng. J. 313 (2017) 928–937, https://doi.org/10.1016/j.cej.2016.10.124.
[45] C. Wang, Y. Wu, J. Lu, J. Zhao, J. Cui, X. Wu, Y. Yan, P. Huo, Bioinspired synthesis of photocatalytic nanocomposite membranes based on synergy of Au-TiO_2 and polydopamine for degradation of tetracycline under visible light, ACS Appl. Mater. Interfaces 9 (2017) 23687–23697, https://doi.org/10.1021/acsami.7b04902.
[46] X. Zhou, C. Shao, S. Yang, X. Li, X. Guo, X. Wang, X. Li, Y. Liu, Heterojunction of g-C_3N_4/BiOI immobilized on flexible electrospun polyacrylonitrile nanofibers: facile preparation and enhanced visible photocatalytic activity for floating photocatalysis, ACS Sustain. Chem. Eng. 6 (2018) 2316–2323, https://doi.org/10.1021/acssuschemeng.7b03760.
[47] F. Li, Z. Yu, H. Shi, Q. Yang, Q. Chen, Y. Pan, G. Zeng, L. Yan, A Mussel-inspired method to fabricate reduced graphene oxide/g-C_3N_4 composites membranes for catalytic decomposition and oil-in-water emulsion separation, Chem. Eng. J. 322 (2017) 33–45, https://doi.org/10.1016/j.cej.2017.03.145.
[48] S.Y. Lee, D. Kang, S. Jeong, H.T. Do, J.H. Kim, Photocatalytic degradation of rhodamine B dye by TiO2 and gold nanoparticles supported on a floating porous polydimethylsiloxane sponge under ultraviolet and visible light irradiation, ACS Omega 5 (2018) 4233–4241, https://doi.org/10.1021/acsomega.9b04127.
[49] A. Singh, S. Chahal, H. Dahiya, A. Goswami, S. Nain, Synthesis of Ag nanoparticle supported graphene/multi-walled carbon nanotube based nanohybrids for photodegradation of toxic dyes, Mater. Express 11 (2021) 936–946, https://doi.org/10.1166/mex.2021.1972.
[50] A. Singh, V. Kaushik, S. Chahal, A. Goswami, S. Nain, Efficient degradation of methylene blue dye and antibacterial performance of shape controlled RuO_2 nanocomposites, ChemistrySelect 6 (2021) 10038–10050, https://doi.org/10.1002/slct.202102546.
[51] F. Persico, M. Sansotera, C.L. Bianchi, C. Cavallotti, W. Navarrini, Photocatalytic activity of TiO_2-embedded fluorinated transparent coating for oxidation of hydrosoluble pollutants in turbid suspensions, Appl. Catal. B Environ. 170–171 (2015) 83–89, https://doi.org/10.1016/j.apcatb.2015.01.033.
[52] E.B. Yazdani, A. Mehrizad, Sonochemical preparation and photocatalytic application of Ag-ZnS-MWCNTs composite for the degradation of Rhodamine B under visible light: experimental design and kinetics modeling, J. Mol. Liq. 255 (2018) 102–112, https://doi.org/10.1016/j.molliq.2018.01.154.
[53] B. Bethi, G.B. Radhika, L.M. Thang, S.H. Sonawane, G. Boczkaj, Photocatalytic decolourization of Rhodamine-B dye by visible light active ZIF-8/$BiFeO_3$ composite, Environ. Sci. Pollut. Res. 30 (2023) 25532–25545, https://doi.org/10.1007/s11356-022-20165-6.
[54] P.M.F. Maciel, N.D.M.N. Fava, A.W. Lamon, P. Fernandez-Ibañez, J.A. Byrne, L. P. Sabogal-Paz, Household water purification system comprising cartridge filtration, UVC disinfection and chlorination to treat turbid raw water, J. Water Process Eng. 43 (2021) 102203, https://doi.org/10.1016/j.jwpe.2021.102203.
[55] H.O.N. Tugaoen, S. Garcia-Segura, K. Hristovski, P. Westerhoff, Challenges in photocatalytic reduction of nitrate as a water treatment technology, Sci. Total Environ. 599 (2017) 1524–1551, https://doi.org/10.1016/j.scitotenv.2017.04.238.